Atmos. Chem. Phys., 25, 16041–16052, 2025 https://doi.org/10.5194/acp-25-16041-2025 © Author(s) 2025. This work is distributed under the Creative Commons Attribution 4.0 License.





Larger than expected organic acid yields from the multi-generation oxidation of petrochemical alkenes

 $\begin{array}{c} \textbf{Baocong Zhao}^{1,2}, \textbf{Luxin Ren}^{1,2}, \textbf{Sihao Lin}^{1,2}, \textbf{Yongpeng Ji}^{1,2}, \textbf{Jiaxin Wang}^{1,2}, \textbf{Tao Ma}^{1,2}, \textbf{Yuemeng Ji}^{1,2}, \\ \textbf{and Taicheng An}^{1,2} \end{array}$

¹Guangdong-Hong Kong-Macao Joint Laboratory for Contaminants Exposure and Health, Guangdong Key Laboratory of Environmental Catalysis and Health Risk Control, Institute of Environmental Health and Pollution Control, Guangdong University of Technology, Guangzhou 510006, China
 ²Guangzhou Key Laboratory of Environmental Catalysis and Pollution Control, Key Laboratory for City Cluster Environmental Safety and Green Development of the Ministry of Education, School of Environmental Science and Engineering, Guangdong University of Technology, Guangzhou 510006, China

Correspondence: Yuemeng Ji (jiym@gdut.edu.cn)

Received: 3 July 2025 – Discussion started: 5 August 2025 Revised: 17 October 2025 – Accepted: 2 November 2025 – Published: 18 November 2025

Abstract. Alkenes are primary pollutants in petrochemical source atmospheres, and their atmospheric chemistry is of great importance for tropospheric ozone and secondary organic aerosol formation. Hence, combining quantum chemical calculations and kinetic modelling, we investigated the oxidation mechanism and kinetics of 2-butene (BU), as one of the most important alkenes, and its impact on the environment. The mechanism results show that OH addition is the dominant pathway for *cis*- and *trans*-isomers of BU, and then the corresponding OH-adducts are attacked by O_2 to produce peroxy radicals, which further react with NO to form acetaldehyde and hydroxyalkyl radicals. Different from the one adopted in current atmospheric models, addition of hydroxyalkyl radicals by O_2 and NO to form acetic acid proceeds with a smaller barrier than that for H-abstraction by O_2 to form acetaldehyde. A lifetime of less than a few hours ($< 4 \, h$) for BU is estimated in the petrochemical regions. Kinetic modelling demonstrates that oxidation of BU is predicted to yield significant amounts of organic acids ($> 56 \, \%$) in the petrochemical areas, larger than those are currently recognized, even in environments with low NO concentrations. Our results reveal that the OH-initiated oxidation of BU contributes importantly to organic acid budgets, particularly in the petrochemical regions, bridging the gap in organic acid budgets.

1 Introduction

Anthropogenic volatile organic compounds (AVOCs) have been associated with climate change, air quality, and environmental impacts via exposure to primary emissions and/or after their photochemical behaviors and multi-generation oxidation (Srivastava et al., 2022; Brook et al., 2010; Chen et al., 2024; Li et al., 2024). The latter leads to secondary air pollution, including secondary organic aerosol (SOA), tropospheric ozone, secondary organic acid, and so on (Peng et al., 2021; Yang et al., 2024; Tan et al., 2019). Automotive emissions of AVOCs have steadily decreased from efforts to control tailpipe emissions in China, and as a result, other

sources of AVOC emissions are growing in relative importance. Among them, petrochemical emissions are appreciable quantities with proportions for 7%-26% of total AVOC emissions. Furthermore, petrochemical emissions exhibit the largest potential of SOA formation ($\sim 23.7\%$) among all industrial emission processes (Wu and Xie, 2018). However, owing to the complex atmospheric chemistry of AVOCs from petrochemical emissions, their reaction mechanisms are uncharacterized, hindering the accurate assessment of their role in air quality and global climate.

Alkenes represent a significant proportion of AVOCs in petrochemical industrial areas (Guo et al., 2022b, a; Henderson et al., 2010; Yang et al., 2023). A field observation re-

vealed that alkenes accounted for 53.7 % \pm 8.5 % of the total VOCs in the Lanzhou petrochemical area, with an average daily concentration of 82.3 ± 13.1 ppb (Yang et al., 2024). Previous studies have shown that multi-generation oxidation of biogenic and anthropogenic alkenes is important to the formation of local free radicals, tropospheric ozone, and SOA (Wu et al., 2021; Wang et al., 2022; Yang et al., 2023; Tan et al., 2024; Huang et al., 2025). For example, the reaction of biogenic alkene, isoprene, with nitrate radicals (NO₃) produces some N-containing monomers and dimers, leading to an estimated yield of organic aerosol mass of approximately $(5\pm2)\%$ (Wu et al., 2021). The gas-phase oxidation of biogenic alkenes (isoprene and monoterpenes) produces abundant semi-volatile organic products, whose second- or latergeneration products are major contributors to SOA (Wang et al., 2018). Recent studies have pointed out that multigeneration oxidation of anthropogenic alkenes contribute to 8 %-20 % of SOA mass (Lee et al., 2022) and about 89 % of O₃ formation (Yang et al., 2024) in the petrochemical regions. Hence, the atmospheric chemistry of alkenes causes significantly secondary pollution to the petrochemical regions. Given the ubiquity of anthropogenic alkenes in petrochemical areas, understanding the multi-generation oxidation mechanisms of anthropogenic alkenes is crucial for accurately predicting their impacts on air quality.

Although multi-generation oxidation of alkenes is believed to be important to SOA and O₃ formation, some studies have highlighted an unignorable source of the multigeneration oxidation for alkenes to secondary organic acids in the troposphere (Link et al., 2021; Srivastava et al., 2023; Wang et al., 2020; Isaacman-Vanwertz et al., 2018; Friedman and Farmer, 2018; Larsen et al., 2001). For example, a previous experimental study has revealed that organic acids obtained by the oxidation of isoprene and α -pinene account for about 28 % of the initial organic carbon (Link et al., 2021). However, a global chemistry-climate model simulation has shown that formic acid, an important class of organic acids in the atmosphere, was underestimated by 2 to 5 times relative to that of satellite observations (Franco et al., 2021). Therefore, current models still highly underestimate ambient concentrations of these acids, indicating that significant sources of organic acid in the atmosphere remain unidentified. Previous studies have identified several missing sources, including primarily from combustion emissions, biogenic emissions, aqueous-phase chemistry of oxygenated VOCs, and photochemical reactions of alkenes (Paulot et al., 2011; Müller et al., 2019; Shaw et al., 2018; Chaliyakunnel et al., 2016; Franco et al., 2021; Link et al., 2021; Parandaman et al., 2018). Therefore, it is interesting to investigate the impact of their photochemistry on the formation of organic acids, to narrow the gap between observed and modelled organic acid concentrations, especially in typical petrochemical areas.

In the present study, we investigated the multi-generation oxidation mechanism and kinetics of 2-butene (BU) initiated by hydroxyl radical (OH) using a combination of quantum chemical calculations and kinetic modelling. BU is a representative alkene in the petrochemical regions, with the concentrations range from 0.5 to 11.4 ppb (Li et al., 2017; Ren et al., 2024; Wang et al., 2022; Zeng et al., 2022). Based on the mechanisms and kinetics, we also applied photochemical box model simulations to study the yields of organic acids from BU. The effects of OH and NO on the reaction mechanisms of BU were evaluated, and the implications of organic acids formation were discussed.

2 Methods

All geometries of the reactants (Rs), pre-reactive complexes, transition states (TSs), intermediates (IMs) and products in this study were fully optimized at the M06-2X/6-311+G(2df,2p) level (Zhao and Truhlar, 2008). Harmonic vibrational frequencies were performed at the same level to check all stationary points either a TS (with only one imaginary frequency) or the minima (without any imaginary frequencies), and to provide zero-point vibrational energy (ZPVE), which is scaled by a factor of 0.967. Intrinsic reaction coordinate (IRC) calculations were carried out at the M06-2X/6-311+G(2df,2p) level to verify that each TS is connected to the desired Rs and products (Fukui, 1981). The single-point energy (SPE) calculations were further refined by the DLPNO-CCSD(T)/aug-cc-pVTZ level (Riplinger et al., 2013) with normal pair natural orbital (NormalPNO) criteria (Liakos et al., 2015) to yield more accurate energetics. T_1 diagnostic values in the DLPNO-CCSD(T) calculations for the IMs and TSs involved in the key reaction pathways were checked for multi-reference character. The T_1 diagnostic values for all checked important species in this work are lower than the threshold value of 0.045, indicating the reliability of applied single reference methods. In all cases, the energies were calculated relative to the corresponding reactants including ZPVE corrections. $\Delta E_a^{\#}$ is defined as the activation energy ($\Delta E_a^{\#} = E_{TS} - E_{Reactant}$), while ΔE_r is defined as the reaction energy ($\Delta E_{\rm r} = E_{\rm Product} - E_{\rm Reactant}$). All above calculations were performed within Gaussian 09 and ORCA 5.0.0 program (Frisch et al., 2009; Neese, 2012). The Multiwfn program and Visual Molecular Dynamics (VMD) were utilized to analyze and visualize the molecular orbitals of relevant species (Humphrey et al., 1996; Lu and Chen, 2012).

The combination of single-conformer and multiconformers approximation was adopted to investigate the reaction mechanism in a cost-effective way of considering the effect of multiple conformers of the reactants and TSs. Based on the single-conformer calculations, the effect of multiple conformers was considered for the crucial reaction step of H-shift reaction of RO₂. The systematic structure scanning method was employed to produce the conformers by the Molclus program (Lu, 2020). The systematic structure scanning was performed by regularly rotating the dihedral angle that determines the conformers of the target molecules. For the target molecules, it yielded 4–256 conformers depending on the complexity of the system. Initial geometry optimizations and single-point electronic energy calculations were performed at the B3LYP/6-31+G(d) level. Subsequently, conformers with electronic energies within 2 kcal mol⁻¹ relative to the lowest-energy conformer were further considered for geometry optimization at the M06-2X/6-311+G(2df,2p) level. On the lowest electronic energy R, intermediate, TS, and product geometries at the M06-2X/6-311+G(2df,2p) level, single-point calculation at the DLPNO-CCSD(T)/aug-cc-pVTZ level was carried out.

The rate constants for the reactions with TSs were calculated using the variational transition state theory (VTST) along with one-dimensional asymmetric Eckart tunnelling correction (Bao and Truhlar, 2017; Eckart, 1930). Besides, the rate constants for the barrierless reactions were calculated by employing the variable-reaction-coordinate variational transition state theory (VRC-VTST) (Bao and Truhlar, 2017). For pathways involving multiple conformers, the rate constants were calculated using multi-conformer transition state theory (MC-TST) (Møller et al., 2016), incorporating data for all conformers obtained from the Molclus program (Lu, 2020). All the kinetics calculations were performed with the KiSThelP 2021 and Polyrate 2017-C programs (Canneaux et al., 2014; Zheng, 2018).

A box-model was used to investigate the formation of organic acids, built using AtChem2 Program (Sommariva et al., 2020) with a chemical mechanism taken from the Master Chemical Mechanism (MCM v3.3.1) (Jenkin et al., 1997; Saunders et al., 2003). The box model was constrained by the initial concentrations of NO, NO₂, BU, and OH as listed in Table S1 in the Supplement (Yang et al., 2024, 2023). The concentration of OH ([OH]) was kept constant throughout the simulation over a 2 h period. More details about the box model simulation are shown in the Supplement.

3 Results and discussion

3.1 OH-Initiated reactions of cis- and trans-BU

In the atmosphere, there exists two stable isomers of BU, i.e., cis-2-butene (cis-BU) and trans-2-butene (trans-BU), which are proven to be ubiquitous and difficult to interconvert (Tu-azon et al., 1998; Wang et al., 2022; Mo et al., 2022). Hence, to systematically assess the photochemistry of BU, we considered the OH-initiated reactions of cis-BU and trans-BU. Figure S1 in the Supplement displays the optimized of structure for all stationary points (SPs) involved in these two reactions at the M06-2X/6-311+G(2df,2p) level. For comparison, other levels, including the B3LYP/, MPW1PW91/, and ω B97X-D/6-311+G(2df,2p) levels, were performed to calculate the geometries (Fig. S2). The structural parameters of all SPs obtained by the four levels are similar, with the largest discrepancies of less than 0.01 Å in bond lengths and 1.70° in bond angles. Hence, the M06-2X level of theory can accu-

rately describe the geometrical information of OH-initiated reactions of *cis*-BU and *trans*-BU.

The potential energy surfaces (PESs) for all possible pathways of the OH-initiated reactions of cis- and trans-BU are presented in Fig. 1. There are two kinds of pathways, i.e., OH-addition (R_{add}) and H-abstraction (R_{abs}). Each pathway has a pre-reactive complex prior to the corresponding TS, which is more stable than the corresponding reactants. As shown in Fig. S1, the C_{2v} symmetry of cis-/trans-BU suggests one OH-addition (cis-/trans-R_{add}) and two H-abstraction (cis-/trans-Rabs) pathways in the cis-/trans-BU reaction systems. For cis-BU, the pathway of Habstraction from $-CH_3$ (cis-R_{abs}1) possesses a lower $\Delta E_a^{\#}$ value of 2.36 kcal mol⁻¹ and a more negative exothermicity of $-30.96 \,\mathrm{kcal}\,\mathrm{mol}^{-1}$ than H-abstraction from $-\mathrm{CH}=\mathrm{group}$ (cis-Rabs2). It is attributed to the smaller bond dissociation energy of C-H bond (D_{298}^0 (C-H)) at the -CH₃ groups relative to that at the -CH= groups in *cis-BU* (Tables S2 and S3). It suggests that the H-abstraction from the -CH₃ group is more favorable than that from the -CH= group. However, OH-addition to C=C double bond (cis-R_{add}1) proceeds via a negative $\Delta E_a^{\#}$ value of $-0.97 \,\mathrm{kcal}\,\mathrm{mol}^{-1}$, which is at least 3 kcal mol⁻¹ smaller than those of H-abstraction pathways, indicating favorable formation of the OH-adduct intermediate (cis-IM_{add}1). Similarly, OH-addition to trans-BU (trans- $R_{add}1$) is also a dominant pathway, but it possesses a more negative $\Delta E_a^{\#}$ value of $-1.33 \, kcal \, mol^{-1}$ than the *cis*- $R_{add}1$ pathway. The interaction region indicator listed in Fig. S3 reveals that OH-addition to the C=C bond of cis-BU exhibits a stronger steric hindrance compared to that of trans-BU, attributed to the van der Waals and steric hindrance interactions between the two -CH₃ groups in cis-TS_{add}1. The larger Mayer bond order of the forming C-O bond in trans-TS_{add}1 (0.251) relative to that in cis-TS (0.192) suggests stronger electronic interactions in the trans-TS_{add}1. This difference, combined with steric hindrance, primarily influences the reactivity of the C=C bond in both cis-BU and trans-BU, leading to the formation of stable OH-adduct intermediates (cisand trans-IMadd 1).

The rate constant of each pathway and the total rate constants (k_{total}) of the OH-initial reactions of cis- and trans-BU were calculated and are summarized in Fig. 2 and Tables S4 and S5, along with comparisons with the available experimental data (Atkinson, 2000; Ohta, 1984). The rate constants were calculated over the temperature range of 240– 340 K, considered from the surface of the earth to the lower troposphere. The total rate constant of each reaction system is obtained by the sum of calculated rate constants for all pathways. There is a negative correlation between k_{total} and temperatures in the temperature range of 240-340 K, attributable to the presence of the pre-reactive complexes (Chen et al., 2022; Giri et al., 2022) and the submerged TSs ($\Delta E_a^{\#} < 0$) (Zádor et al., 2009) in the OH-addition pathways. Our calculated rate constants at the DLPNO/aug-ccpVTZ//M06-2X/6-311+G(2df,2p) level also compare favor-

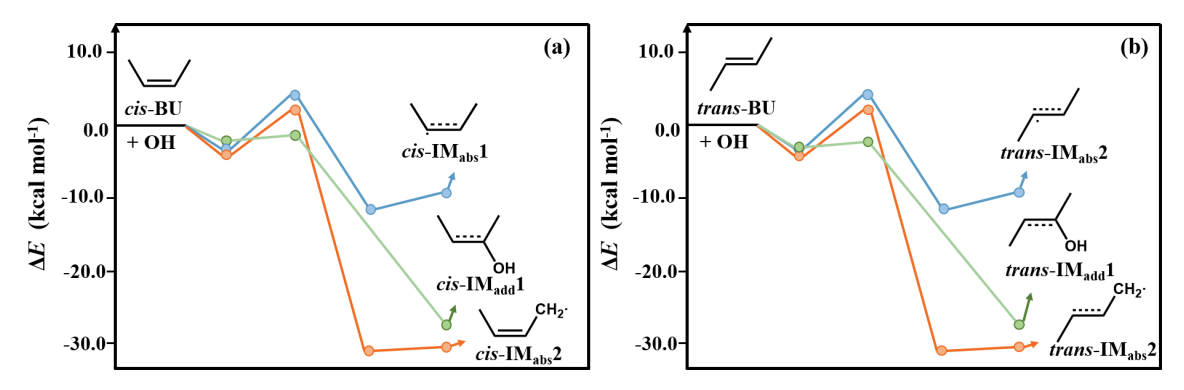


Figure 1. Potential energy surfaces (PESs) for the OH-initiated reactions of (a) cis-BU and (b) trans-BU with OH (unit: kcal mol⁻¹).

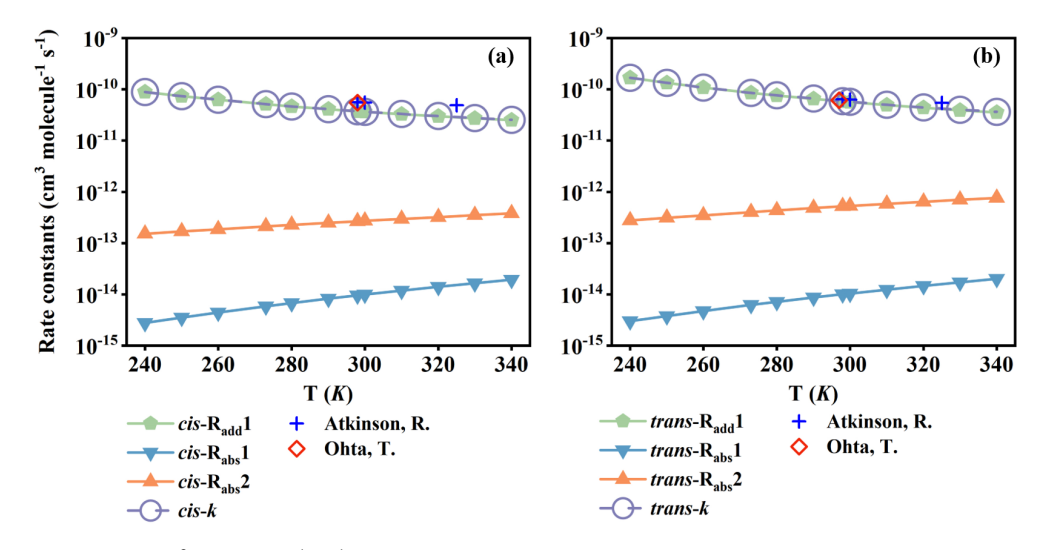


Figure 2. The rate constants (cm 3 molecule $^{-1}$ s $^{-1}$) of (a) *cis*-BU and (b) *trans*-BU with OH against the temperature range of 240–340 K. The experimental rate constants are from Atkinson (2000) and Ohta (1984), respectively.

ably with the available experimental data. For example, the rate constant of the trans-BU+OH reaction at 298 K is $5.85 \times 10^{-11} \, \mathrm{cm^3}$ molecule $^{-1} \, \mathrm{s^{-1}}$, in lines with the experimental values of $(5.40 \pm 0.02) \times 10^{-11} \, \mathrm{cm^3}$ molecule $^{-1} \, \mathrm{s^{-1}}$ reported by Atkinson (2000) and $(6.09 \pm 0.3) \times 10^{-11}$ obtained by Ohta (1984). Hence, the DLPNO-CCSD(T)/aug-cc-pVTZ//M06-2X/6-311+G(2df,2p) method provides a reliable description for the kinetics of the OH-initial reactions of cis-BU and trans-BU.

Tables S4 and S5 list the temperature dependences of the branching ratios (Γ) over the temperature range from 240 to 340 K. For *cis*-BU, the rate constant of OH-addition pathway is at least two orders of magnitude higher than those of the corresponding H-abstraction pathways. At 340 K, the OH-addition pathway accounts for 98.4% of the total reaction, this fraction increases to 99.8% when the temperature is lowered to 240 K. The contribution of OH-addition pathway to the total rate constant is more than 99% in the whole measured temperature ranges. Similarly, for *trans*-BU, the OH-addition pathway is also of major importance. Ar-

rhenius expressions are derived to be $k_{\rm total}(cis\text{-BU}+\text{OH}) = 1.23 \times 10^{-12} \exp(1021.32/T)$ and $k_{\rm total}(trans\text{-BU}+\text{OH}) = 8.90 \times 10^{-13} \exp(1251.48/T)$ over the temperature range of 240–340 K. From the calculated Arrhenius expressions, the activation energies of the cis- and trans-BU reaction systems are deduced to be -2.03 and -2.49 kcal mol⁻¹, respectively. These negative activation energy values indicate that the OH-initiated reactions of cis- and trans-BU are kinetically favored in the troposphere, to rapidly form the OH-adduct intermediates.

3.2 Subsequent reactions of the OH-adduct intermediates

The OH-adduct intermediates, i.e., cis- and trans-IM_{add}1, proceed via three competitive pathways including reaction with O₂ (R3), isomerization (R4), and decomposition (R5). A Schematic PES presented in Fig. S4 reveals that the TSs of cis- and trans-R3 are not identified, but there are TSs for R4 and R5 pathways with the $\Delta E_a^{\#}$ values more than

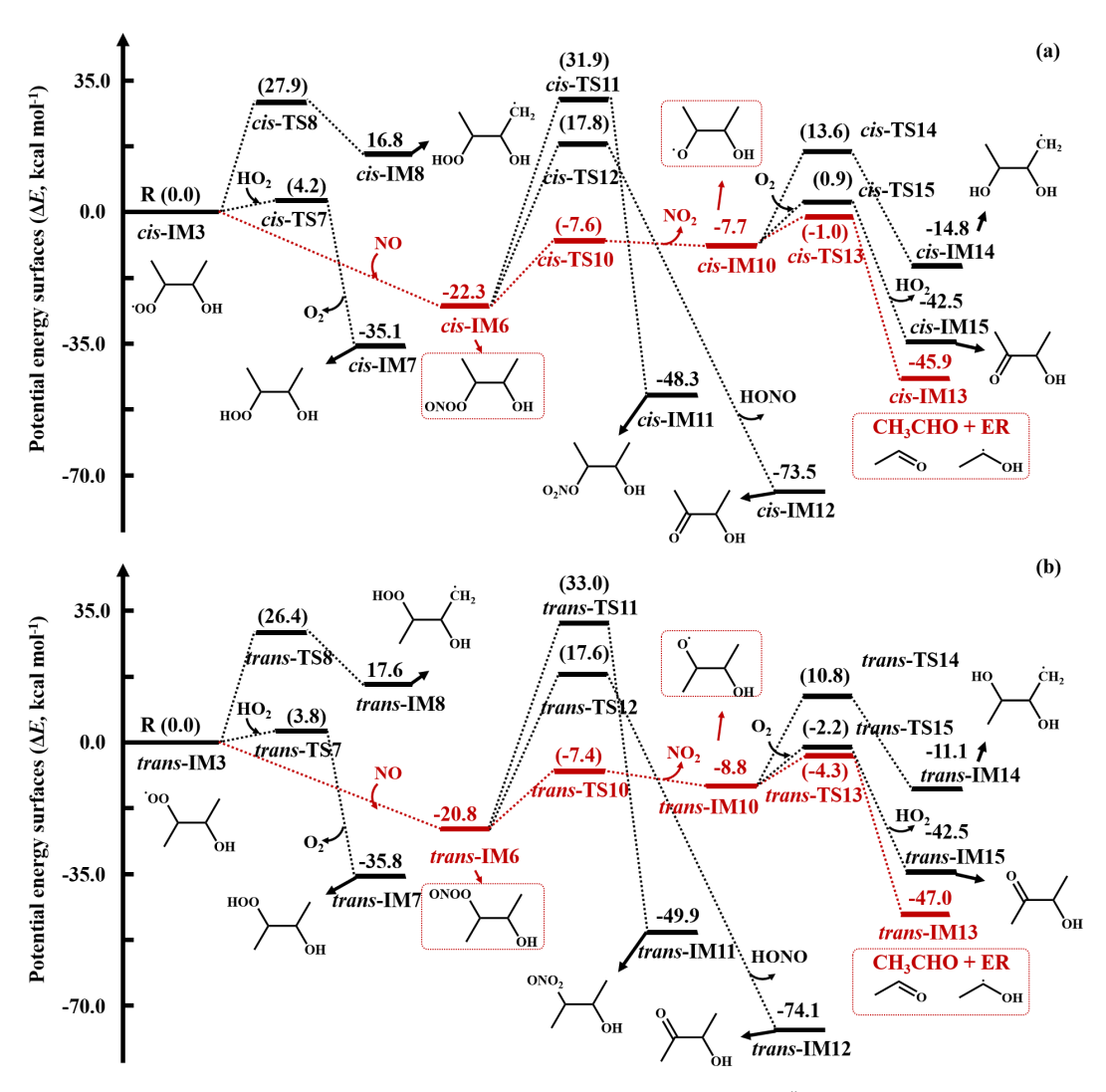


Figure 3. PESs of the reaction of (a) cis-IM3 and (b) trans-IM3. The number denotes the ΔE_a^{\dagger} and ΔE_{r} for each reaction step.

 $30.0\,\mathrm{kcal\,mol^{-1}}$. The calculated rate constants of R4 and R5 pathways are 7.3×10^{-13} and $2.6\times10^{-11}\,\mathrm{s^{-1}}$ in the *cis*- and *trans*-BU reaction systems (Table S6), which are 18-20 orders of magnitude smaller than that of R3 ($6.0\times10^{-11}\,\mathrm{cm^3}$ molecule⁻¹ s⁻¹, corresponding to an equivalent first-order rate constant of $3.0\times10^7\,\mathrm{s^{-1}}$). Considering the branching ratios among the three pathways, about 99 % of both *cis*- and *trans*-IM_{add}1 react with O₂ to form peroxy radicals (*cis*-/*trans*-RO₂), which further propagate the oxidation.

For cis-RO₂, attacked by NO (cis-R6) or HO₂ radical (cis-R7) forms the peroxy nitrite (cis-RO₂NO) or the hydroperoxide (cis-ROOH). Alternatively, there exists the autoxidation of cis-RO₂, which proceeds via two-step reactions, i.e., a H-shift reaction (cis-R8) followed by an O₂-addition (cis-R9), with the high $\Delta E_a^{\#}$ value and the small rate constant (Figs. S7 and S8). Similarly, the reaction with HO₂ radical also proceeds via a TS with the $\Delta E_a^{\#}$ value of 4.20 kcal mol⁻¹ (Fig. S6). However, the association reaction of cis-RO₂ with

NO is barrierless and exothermic (Figs. 3 and S5), and the corresponding equivalent first-order rate constant is 1.1 s⁻¹, which is at least five orders of magnitude higher than those of *cis*-R7 and *cis*-R8 pathways (Tables S7–S11).

As shown in Fig. S8, the reaction of cis-RO₂ with HO₂ is competitive in the troposphere only if HO₂ concentration exceeds 40 ppt, which is the maximum atmospheric concentration. It implies that the cis-RO₂NO is the dominant product from cis-RO₂. Subsequently, there are three reaction pathways of cis-RO₂NO, i.e., NO₂-elimination (cis-R10), intramolecular isomerization (cis-R11), and dissociation (cis-R12). The $\Delta E_a^{\#}$ values of cis-R11 and cis-R12 are 54.23 and 38.35 kcal mol⁻¹ (Fig. 3), respectively, which are 26.36 kcal mol⁻¹ larger than that of cis-R10. It indicates that the formation of organic nitrates (cis-ON), acetoin (CH₃CH(OH)C(=O)CH₃), and HONO is of minor importance. The calculated HONO yield is < 1%, indicating the negligible formation, in contrast to the

yield of 50% for 1-butene under high-NO_x conditions reported by Chen et al. (Chen et al., 2021). The discrepancy is attributed to the characteristic of structure, i.e., the distinct β -hydrogen availability of the two alkenes. As shown in Fig. 3, the favorably produced alkoxy radical (cis-RO) via cis-R10 then undergoes dissociation (cis-R13), isomerization (cis-R14), and H-abstraction (cis-R15) to yield acetaldehyde (CH₃CHO) and hydroxyalkyl radicals (CH₃CHOH), CH₃CH(OH)CH(OH)CH₂ radical, and acetoin (CH₃C(=O)CH(OH)CH₃), respectively. The cis-R13 pathway possesses a smaller $\Delta E_a^{\#}$ value of 6.51 kcal mol⁻¹ and a larger rate constant of 1.10×10^8 s⁻¹ at 298 K relative to the cis-R14 and cis-R15 pathways (Table S12), indicating a major importance to form CH₃CHO and CH₃CHOH.

Similarly, as shown in Fig. S5, the subsequent reactions of trans-RO2 involve three essential steps: (i) the association with NO to form trans-RO₂NO, (ii) the NO₂-elimination of trans-RO2NO to produce trans-RO, and (iii) the dissociation of trans-RO to yield CH₃CHO and CH₃CHOH radical. However, the differences between the subsequent reactions of cis-IM_{add}1 and trans-IM_{add}1 are reflected in the lower reaction energy barriers and the larger rate constants of trans-IM_{add}1. For example, the $\Delta E_a^{\#}$ value of trans-R12 pathway is 11.99 kcal mol⁻¹, which is 2.6 kcal mol⁻¹ lower than that of cis-R12 pathway, and the corresponding rate constant of trans-R12 pathway is six times larger than that of cis-R12 pathway. It is attributed to a stronger steric hindrance in subsequent reactions of cis-IM_{add}1 relative to trans-IM_{add}1. Therefore, CH₃CHO and CH₃CHOH radicals are more rapidly produced from trans-BU relative to cis-BU in the atmosphere.

3.3 The fate of BU

According to the previous study (Da Silva et al., 2009; Zádor et al., 2009), CH₃CHOH• radical (ER) undergoes a step-wise O₂-addition/HO₂-elimination mechanism (R16) via ER-O2 formation, to form CH3CHO and HO2 radical. The formation of ER-O2 is an exothermic process with the $\Delta E_{\rm r}$ of $-34.11\,{\rm kcal\,mol}^{-1}$, which supports to overcome the $\Delta E_a^{\#}$ value of 11.27 kcal mol⁻¹ (Figs. 4 and S9). However, under the petrochemical conditions, ER-O2 readily react with NO, which is abundant in polluted areas, forming ER-O₂NO, because this reaction is a barrierless and largely exothermic with the $\Delta E_a^{\#}$ value of $-24.16 \,\mathrm{kcal} \,\mathrm{mol}^{-1}$ (R17). Subsequent decomposition of ER-O₂NO (R19) possesses a $\Delta E_a^{\#}$ value of 13.69 kcal mol⁻¹, which can be overcome because the excess energy (-24.16 kcal mol⁻¹) from ER-O2NO formation, leading to the formation of alkoxy radical (ER-O) and NO2. ER-O reacts with O2 (R20) to produce acetic acid (CH₃COOH) and HO₂ radical, with the $\Delta E_a^{\#}$ and ΔE_r values of 5.40 and -48.13 kcal mol⁻¹, respectively. To elucidate the significance of acid formation pathway in petrochemical regions, the kinetic data were investigated and listed in Table S13. The rate constant for CH₃CHO and HO₂ formation is $2.03 \times 10^{-11} \,\mathrm{cm}^3 \,\mathrm{molecule}^{-1} \,\mathrm{s}^{-1}$ at 298 K, which is slightly smaller than that for ER-O and NO_2 formation $(4.79 \times 10^{-11} \text{ cm}^3 \text{ molecule}^{-1} \text{ s}^{-1})$. Furthermore, the predicted branching ratios forming CH₃CHO and CH₃COOH are 29.7 % and 69.4 %, respectively, which requires to further assess the contribution of BU to organic acids in the atmosphere. Furthermore, we predict a minor pathway via $RO_2 + NO$ reaction to form organic nitrate, consistent with the work by Muthuramu et al. (1993) for a small yield for the formation of organic nitrate from cis-BU $(3.7\% \pm 0.9\%)$. In addition, we also evaluate the tropospheric lifetimes (τ) for cis-BU and trans-BU at different [OH] levels. The gas-phase OH oxidation lifetimes were estimated using $\tau = 1/(k_{\text{total}}[\text{OH}])$, where k_{total} and [OH] are the total rate constant and OH concentration, respectively. As shown in Table S14, the τ values are 9.29 and 5.93 h for cis-BU and trans-BU, respectively, under the remote areas with the [OH] of 8×10^5 molecule cm⁻³, which are higher than those of the corresponding lifetimes under the petrochemical regions with the [OH] of 1×10^7 molecule cm⁻³. The short τ value of BUs in the petrochemical regions indicate that they are more readily oxidized, implying a more significant environmental impact in these regions compared to urban regions. The τ values of *cis*- and *trans*-BU are further shortened to be 2.70 and 1.62 h as the temperature drops to 273 K in the petrochemical regions. Given that organic acids are more conducive to atmospheric new particle formation and growth under low-temperature conditions (Peng et al., 2021), it is essential to focus on the contribution of the BU oxidation in the petrochemical regions to the formation of organic acids at low temperatures.

3.4 Rate of CH₃COOH formation

To evaluate the impact of our established mechanisms on the formation of organic acids in the petrochemical regions, a box model simulation was performed to quantify the production rate $(r_{\text{CH}_3\text{COOH}})$ and yield $(Y_{\text{CH}_3\text{COOH}})$ of CH₃COOH by using the MCM v3.3.1 coupled with the AtChem2 box model. For comparison, the corresponding simulation under the traditional mechanism of CH₃COOH formation in MCM v3.3.1 was also carried out. All the simulations were conducted using the measured mixing ratios of BUs, OH, and NO in a typical petrochemical industrial region, and all the settings were posted in Table S1 (Yang et al., 2024). It is evident from Figs. 5 and S10 that the $r_{\text{CH}_3\text{COOH}}$ values corrected with our proposed mechanism exhibit a significant increase of more than ten times under typical petrochemical conditions, where the concentrations of [OH] and NO ([NO]) are 2×10^6 molecule cm⁻³ and 10 ppb $(2.5 \times 10^{11} \, \text{molecule cm}^{-3})$, respectively. Even when [OH] and [NO] decrease, the $r_{\text{CH}_3\text{COOH}}$ values are also increased by more than five times. Large production rates of CH₃COOH correspond to the high Y_{CH₃COOH} values, for example, the $Y_{\text{CH}_3\text{COOH}}$ value in cis-BU + OH reaction with

Figure 4. Schematic representation of the preferred pathways of the *cis*-BU+OH reactions leading to formation of acetaldehyde (CH₃CHO) and acetic acid (CH₃COOH). Values of branching ratio are shown in black.

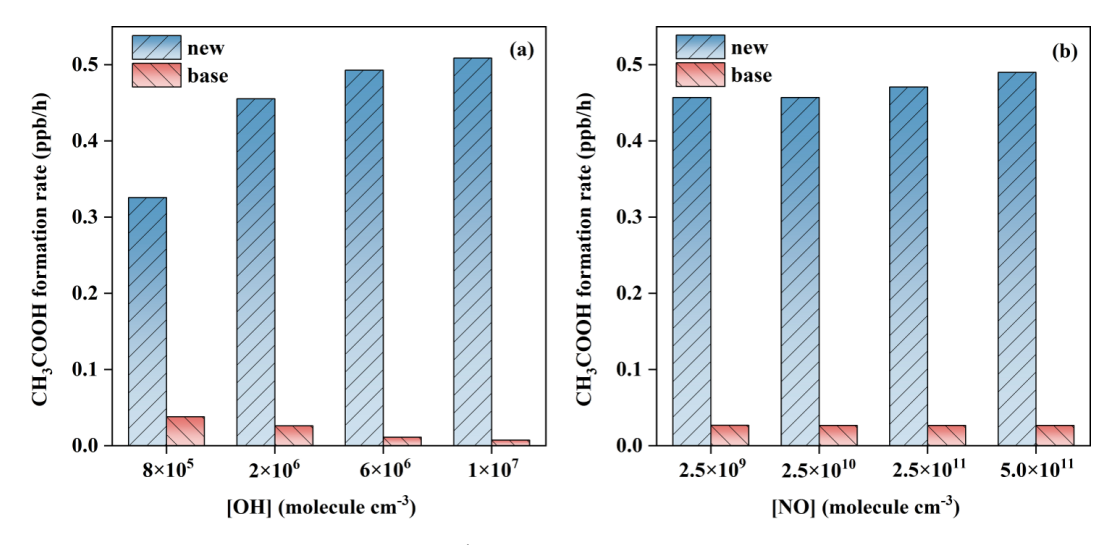


Figure 5. Mean formation rate of CH_3COOH (unit: $ppbh^{-1}$) from the cis-BU + OH reactions as a function of (a) OH concentration ([OH]) and (b) NO concentration ([NO]) under the petrochemical region conditions. The comparison is made between the MCMv3.3.1 and the new mechanism.

57% is more than ten times higher than that without our proposed mechanism under the typical petrochemical conditions. Hence, the photooxidation of *cis-/trans-BU* corrected by our proposed mechanisms has a significant impact on the formation of organic acids in the petrochemical source regions, with particularly pronounced effects on the formation of small-molecule gaseous organic acids.

To further assess the atmospheric regions where the photochemistry of BU will have significance, we also calculated the $r_{\text{CH}_3\text{COOH}}$ values under the varying [OH] and [NO]

corresponding to the atmospheric conditions (Figs. 5 and S10) (Tan et al., 2019). In a high [NO] condition of 4.9×10^{10} molecule cm⁻³ with the [OH] of 6×10^6 molecule cm⁻³, the $r_{\text{CH}_3\text{COOH}}$ values are 0.51 and 0.47 ppb h⁻¹ in cis-BU + OH and trans-BU + OH reactions, which are at least 55% larger than those with the [OH] of 8×10^5 molecule cm⁻³, respectively. Even in a low [NO] condition of 2.5×10^9 molecule cm⁻³, the $r_{\text{CH}_3\text{COOH}}$ values in two reactions are also significantly regulated by the atmospheric [OH]. However, there is little effect of [NO] on the $r_{\text{CH}_3\text{COOH}}$ values.

For example, at the same [OH] of 2×10^6 molecule cm⁻³, the $r_{\text{CH}_3\text{COOH}}$ value in cis-BU + OH reaction is $0.49 \text{ ppb}\,\text{h}^{-1}$ at the [NO] of 5.0×10^{11} molecule cm⁻³, while in the [NO] of 2.5×10^9 molecule cm⁻³, the $r_{\text{CH}_3\text{COOH}}$ value is only decreased by 7%. Combined with the mechanism results, the yield of organic acid from the BU + OH reaction is regulated by the atmospheric OH concentration. Therefore, under both typical petrochemical source region conditions and general atmospheric conditions, cis-BU + OH and trans-BU + OH reactions can form CH₃COOH through the subsequent oxidation of CH₃CHOH radicals, exhibiting unexpectedly high formation rates during daylight hours.

4 Conclusions and atmospheric implications

AVOCs have profound impacts on air quality, human health and climate, and BU is the major AVOCs emitted from the petrochemical regions. Hence, from combined quantum chemical calculations and photochemical box model simulations, this study provides a systematic insight into the multigeneration oxidation mechanisms, kinetics, and atmospheric fate of BU and its contribution to the formation of organic acid. The initial reactions of both the cis- and trans-isomers of BU readily involve OH addition to the C=C double bond, yielding the corresponding OH-adducts. Subsequent reactions proceed via O2 addition, NO-association, NO2elimination, and further decomposition to produce CH₃CHO and CH₃CHOH radical. CH₃CHOH radical is converted into CH₃COOH and HO₂ radical, facilitated by O₂ and NO through the pathways of O₂ addition, NO-association, NO₂elimination, and H-abstraction. Our mechanism highlights that the rapid and irreversible reaction of CH₃CHOH• with O₂ and NO is a key mechanistic step in the formation of CH₃COOH, which is one of the most favorable products, with a yield of 57 %. However, previous experimental studies on the OH-initiated oxidation of BU obtained a low yield of CH₃COOH (< 10 %) (Atkinson, 1997; Muthuramu et al., 1993). Given the rapid partitioning of gas CH₃COOH into the liquid phase in the experimental environment (Franco et al., 2021), the measured yield likely corresponds to the lower experimental limit.

This study further reveals that the multi-generation oxidation of BU in the petrochemical environment, may be particularly important for organic acid formation. Using our calculated kinetics data, we estimate a lifetime of less than 4 h for BU in the petrochemical environment, indicating that BU are rapidly oxidized following the local emission. By adding our established mechanisms to the photochemical box model simulations, our calculated formation rates and yields of CH₃COOH are at least 10 times higher than those from the traditional mechanism. Besides, the impact of OH concentrations on the formation rate of CH₃COOH is greater than that of NO concentrations. That is, the formation rate of CH₃COOH rapidly drops, as OH concentrations decrease.

This highlights the dominant role of OH radicals in the initial oxidation steps of multi-step oxidation processes. With the increasing oxidative capacity and decreasing nitrogen oxides (NO_x) abundance in polluted areas (Newland et al., 2021), further study is needed to explore the impacts of these factors on the multi-generation oxidation reactions of alkenes.

Contrary to the consensus that the complex multigeneration oxidation of alkenes primarily contributes to the formation of low-volatility products, we discovered that the multi-generation oxidation of BU can unexpectedly contribute to the formation of organic acids. The unexpected production of organic acids can not only help to explain the missing source of organic acids but also affect the acidity of atmospheric precipitation, especially for the petrochemical region atmosphere. In the atmosphere, we predict that the multi-generation oxidation of alkenes during the daytime will produces CH_3COOH at a rate of 10.4 ppb h^{-1} (Fig. S10), which can be comparable with the simulated source from the photochemical reaction of biogenic alkenes (Paulot et al., 2011). Therefore, the mechanism for the formation of organic acids from BU isomers established by this study is more significant than previously recognized, particularly in the petrochemical regions with the high emissions of BU isomers. Further investigation is warranted into the multigeneration oxidation of AVOCs, as well as their impacts on the formation of organic acids and the environment.

Data availability. The data are accessible by contacting the corresponding author (jiym@gdut.edu.cn).

Supplement. The following information is provided in the Supplement: the comparison of the geometries of cis- and transisomers of BU calculated at the M06-2X/6-311+G(2df,2p) level of theory and other levels including B3LYP/6-311+G(2df,2p), MPW1PW91/6-311+G(2df,2p), and ω B97X-D/6-311+G(2df,2p); the interaction region indicator analyses of of cis-TS_{add}1 and trans-TS_{add}1; rate constants of each elementary pathway involved in the reaction of cis-BU + OH and trans-BU + OH; PESs for the subsequent reactions of cis- and trans-isomers of OH adduct, involving the bimolecular reactions with O2, NO, and HO2, and the unimolecular reactions of isomerization and dissociation; geometries of all stationary points; mean formation rate of CH₃COOH from the trans-BU + OH reactions; parameter settings and simulation results of the AtChem2 model. The supplement related to this article is available online at https://doi.org/10.5194/acp-25-16041-2025supplement.

Author contributions. YJ and BZ designed the research; YJ, BZ, LR and SL performed the research; BZ, YJ, LR, JW, TM and TA analyzed the data; YJ and BZ wrote the paper; LR, JW, YJ, TM and TA reviewed and edited the paper.

Competing interests. The contact author has declared that none of the authors has any competing interests.

Disclaimer. Publisher's note: Copernicus Publications remains neutral with regard to jurisdictional claims made in the text, published maps, institutional affiliations, or any other geographical representation in this paper. While Copernicus Publications makes every effort to include appropriate place names, the final responsibility lies with the authors. Views expressed in the text are those of the authors and do not necessarily reflect the views of the publisher.

Acknowledgements. We thank Hai Guo and Yu Yang (The Hong Kong Polytechnic University, China) and co-workers for coordinating the intensive sampling campaign in the petrochemical industrial area. The study was supported by National Natural Science Foundation of China (42020104001, U25A20825, 42577431, and 42077189), Guangdong Basic and Applied Basic Research Foundation (2025A1515011379), Technology Elite Navigation Project of Guangzhou (2025A04J7038), and Guang-dong Provincial Key R&D Program (2022-GDUT-A0007).

Financial support. This work was financially supported by National Natural Science Foundation of China (grant nos. 42020104001, U25A20825, 42577431, and 42077189), Guangdong Basic and Applied Basic Research Foundation (grant no. 2025A1515011379), Technology Elite Navigation Project of Guangzhou (grant no. 2025A04J7038), and Guang-dong Provincial Key R&D Program (grant no. 2022-GDUT-A0007).

Review statement. This paper was edited by Benjamin A. Nault and reviewed by two anonymous referees.

References

- Atkinson, R.: Atmospheric reactions of alkoxy and β -hydroxyalkoxy radicals, Int. J. Chem. Kinet., 29, 99–111, https://doi.org/10.1002/(SICI)1097-4601(1997)29:2<99::AID-KIN3>3.0.CO;2-F, 1997.
- Atkinson, R.: Atmospheric chemistry of VOCs and NO_x, Atmos. Environ., 34, 2063–2101, https://doi.org/10.1016/S1352-2310(99)00460-4, 2000.
- Bao, J. L. and Truhlar, D. G.: Variational transition state theory: theoretical framework and recent developments, Chemical Society Reviews, 46, 7548–7596, https://doi.org/10.1039/C7CS00602K, 2017.
- Brook, R. D., Rajagopalan, S., Pope, C. A., Brook, J. R., Bhatnagar, A., Diez-Roux, A. V., Holguin, F., Hong, Y., Luepker, R. V., Mittleman, M. A., Peters, A., Siscovick, D., Smith, S. C., Whitsel, L., and Kaufman, J. D.: Particulate Matter Air Pollution and Cardiovascular Disease, Circulation, 121, 2331–2378, https://doi.org/10.1161/CIR.0b013e3181dbece1, 2010.
- Canneaux, S., Bohr, F., and Henon, E.: KiSThelP: A program to predict thermodynamic properties and rate constants from

- quantum chemistry results, J. Comput. Chem., 35, 82–93, https://doi.org/10.1002/jcc.23470, 2014.
- Chaliyakunnel, S., Millet, D. B., Wells, K. C., Cady-Pereira, K. E., and Shephard, M. W.: A Large Underestimate of Formic Acid from Tropical Fires: Constraints from Space-Borne Measurements, Environ. Sci. Technol., 50, 5631–5640, https://doi.org/10.1021/acs.est.5b06385, 2016.
- Chen, L., Huang, Y., Xue, Y., Jia, Z. and Wang, W.: Atmospheric oxidation of 1-butene initiated by OH radical: Implications for ozone and nitrous acid formations, Atmos. Environ., 244, 118010, https://doi.org/10.1016/j.atmosenv.2020.118010, 2021.
- Chen, L., Huang, Y., Xue, Y., Jia, Z., and Wang, W.: Kinetic and Mechanistic Investigations of OH-Initiated Atmospheric Degradation of Methyl Butyl Ketone, J. Phys. Chem. A, 126, 2976– 2988, https://doi.org/10.1021/acs.jpca.2c01126, 2022.
- Chen, Q., Miao, R., Geng, G., Shrivastava, M., Dao, X., Xu, B., Sun, J., Zhang, X., Liu, M., Tang, G., Tang, Q., Hu, H., Huang, R.-J., Wang, H., Zheng, Y., Qin, Y., Guo, S., Hu, M., and Zhu, T.: Widespread 2013–2020 decreases and reduction challenges of organic aerosol in China, Nat. Commun., 15, 4465, https://doi.org/10.1038/s41467-024-48902-0, 2024.
- Da Silva, G., Bozzelli, J. W., Liang, L., and Farrell, J. T.: Ethanol Oxidation: Kinetics of the α -Hydroxyethyl Radical + O₂ Reaction, J. Phys. Chem. A, 113, 8923–8933, https://doi.org/10.1021/jp903210a, 2009.
- Eckart, C.: The Penetration of a Potential Barrier by Electrons, Physical Review, 35, 1303–1309, https://doi.org/10.1103/PhysRev.35.1303, 1930.
- Franco, B., Blumenstock, T., Cho, C., Clarisse, L., Clerbaux, C., Coheur, P. F., De Mazière, M., De Smedt, I., Dorn, H. P., Emmerichs, T., Fuchs, H., Gkatzelis, G., Griffith, D. W. T., Gromov, S., Hannigan, J. W., Hase, F., Hohaus, T., Jones, N., Kerkweg, A., Kiendler-Scharr, A., Lutsch, E., Mahieu, E., Novelli, A., Ortega, I., Paton-Walsh, C., Pommier, M., Pozzer, A., Reimer, D., Rosanka, S., Sander, R., Schneider, M., Strong, K., Tillmann, R., Van Roozendael, M., Vereecken, L., Vigouroux, C., Wahner, A., and Taraborrelli, D.: Ubiquitous atmospheric production of organic acids mediated by cloud droplets, Nature, 593, 233–237, https://doi.org/10.1038/s41586-021-03462-x, 2021.
- Friedman, B. and Farmer, D. K.: SOA and gas phase organic acid yields from the sequential photooxidation of seven monoterpenes, Atmos. Environ., 187, 335–345, https://doi.org/10.1016/j.atmosenv.2018.06.003, 2018.
- Frisch, M. J., Trucks, G. W., Schlegel, H. B., Scuseria, G. E., Robb, M. A., Cheeseman, J. R., Scalmani, G., Barone, V., Mennucci, B., Petersson, G. A., Nakatsuji, H., Caricato, M., Li, X., Hratchian, H. P., Izmaylov, A. F., Bloino, J., Zheng, G., Sonnenberg, J. L., Hada, M., Ehara, M., Toyota, K., Fukuda, R., Hasegawa, J., Ishida, M., Nakajima, T., Honda, Y., Kitao, O., Nakai, H., Vreven, T., Montgomery, Jr., J. A., Peralta, J. E., Ogliaro, F., Bearpark, M., Heyd, J. J., Brothers, E., Kudin, K. N., Staroverov, V. N., Keith, T., Kobayashi, R., Normand, J., Raghavachari, K., Rendell, A., Burant, J. C., Iyengar, S. S., Tomasi, J., Cossi, M., Rega, N., Millam, J. M., Klene, M. Knox, J. E., Cross, J. B., Bakken, V., Adamo, C., Jaramillo, J., Gomperts, R., Stratmann, R. E., Yazyev, O., Austin, A. J., Cammi, R., Pomelli, C., Ochterski, J. W., Martin, R. L., Morokuma, K., Zakrzewski, V. G., Voth, G. A., Salvador, P., Dannenberg, J. J., Dapprich, S., Daniels, A. D., Farkas, Ö., Foresman, J. B., Ortiz,

- J. V., Cioslowski, J. and Fox, D. J.: Gaussian 09, Revision D.01, Gaussian, Inc., Wallingford, CT, http://www.gaussian.com (last access: 1 July 2025), 2009.
- Fukui, K.: The path of chemical reactions the IRC approach, Acc. Chem. Res., 14, 363–368, https://doi.org/10.1021/ar00072a001, 1981.
- Giri, B. R., V.-T. Mai, T., Assali, M., Nguyen, T. T. D., Nguyen, H. T., Szőri, M., Huynh, L. K., Fittschen, C., and Farooq, A.: Reaction kinetics of 1,4-cyclohexadienes with OH radicals: an experimental and theoretical study, Phys. Chem. Chem. Phys., 24, 7836–7847, https://doi.org/10.1039/D1CP04964J, 2022.
- Guo, W., Chen, Q., Yang, Y., Zhang, Y., Liu, X., Zhang, R., Zhu, Y., Li, G., Liu, P., and Chen, M.: Investigating the mechanism of morning ozone concentration peaks in a petrochemical industrial city, Atmos. Environ., 270, 118897, https://doi.org/10.1016/j.atmosenv.2021.118897, 2022a.
- Guo, W., Yang, Y., Chen, Q., Zhu, Y., Zhang, Y., Zhang, Y., Liu, Y., Li, G., Sun, W., and She, J.: Chemical reactivity of volatile organic compounds and their effects on ozone formation in a petrochemical industrial area of Lanzhou, Western China, Sci. Total Environ., 839, 155901, https://doi.org/10.1016/j.scitotenv.2022.155901, 2022b.
- Henderson, B. H., Jeffries, H. E., Kim, B.-U., and Vizuete, W. G.: The Influence of Model Resolution on Ozone in Industrial Volatile Organic Compound Plumes, J. Air Waste Manag. Assoc., 60, 1105–1117, https://doi.org/10.3155/1047-3289.60.9.1105, 2010.
- Huang, R.-J., Li, Y. J., Chen, Q., Zhang, Y., Lin, C., Chan, C. K., Yu, J. Z., de Gouw, J., Tong, S., Jiang, J., Wang, W., Ding, X., Wang, X., Ge, M., Zhou, W., Worsnop, D., Boy, M., Bilde, M., Dusek, U., Carlton, A. G., Hoffmann, T., McNeill, V. F., and Glasius, M.: Secondary organic aerosol in urban China: A distinct chemical regime for air pollution studies, Science, 389, eadq2840, https://doi.org/10.1126/science.adq2840, 2025.
- Humphrey, W., Dalke, A., and Schulten, K.: VMD: Visual molecular dynamics, Journal of Molecular Graphics, 14, 33–38, https://doi.org/10.1016/0263-7855(96)00018-5, 1996.
- Isaacman-VanWertz, G., Massoli, P., O'Brien, R., Lim, C., Franklin, J. P., Moss, J. A., Hunter, J. F., Nowak, J. B., Canagaratna, M. R., Misztal, P. K., Arata, C., Roscioli, J. R., Herndon, S. T., Onasch, T. B., Lambe, A. T., Jayne, J. T., Su, L., Knopf, D. A., Goldstein, A. H., Worsnop, D. R., and Kroll, J. H.: Chemical evolution of atmospheric organic carbon over multiple generations of oxidation, Nat. Chem., 10, 462–468, https://doi.org/10.1038/s41557-018-0002-2, 2018.
- Jenkin, M. E., Saunders, S. M., and Pilling, M. J.: The tropospheric degradation of volatile organic compounds: a protocol for mechanism development, Atmos. Environ., 31, 81–104, https://doi.org/10.1016/S1352-2310(96)00105-7, 1997.
- Larsen, B. R., Di Bella, D., Glasius, M., Winterhalter, R., Jensen, N. R., and Hjorth, J.: Gas-Phase OH Oxidation of Monoterpenes: Gaseous and Particulate Products, J. Atmos. Chem., 38, 231–276, https://doi.org/10.1023/A:1006487530903, 2001.
- Lee, Y. R., Huey, L. G., Tanner, D. J., Takeuchi, M., Qu, H., Liu, X., Ng, N. L., Crawford, J. H., Fried, A., Richter, D., Simpson, I. J., Blake, D. R., Blake, N. J., Meinardi, S., Kim, S., Diskin, G. S., Digangi, J. P., Choi, Y., Pusede, S. E., Wennberg, P. O., Kim, M. J., Crounse, J. D., Teng, A. P., Cohen, R. C., Romer, P. S., Brune, W., Wisthaler, A., Mikoviny, T., Jimenez,

- J. L., Campuzano-Jost, P., Nault, B. A., Weinheimer, A., Hall, S. R., and Ullmann, K.: An investigation of petrochemical emissions during KORUS-AQ: Ozone production, reactive nitrogen evolution, and aerosol production, Elem. Sci. Anth., 10, https://doi.org/10.1525/elementa.2022.00079, 2022.
- Li, B., Ho, S. S. H., Xue, Y., Huang, Y., Wang, L., Cheng, Y., Dai, W., Zhong, H., Cao, J., and Lee, S.: Characterizations of volatile organic compounds (VOCs) from vehicular emissions at roadside environment: The first comprehensive study in Northwestern China, Atmos. Environ., 161, 1–12, https://doi.org/10.1016/j.atmosenv.2017.04.029, 2017.
- Li, C., Martin, R. V., and van Donkelaar, A.: Understanding Reductions of PM_{2.5} Concentration and Its Chemical Composition in the United States: Implications for Mitigation Strategies, ACS ES&T Air, 1, 637–645, https://doi.org/10.1021/acsestair.4c00004, 2024.
- Liakos, D. G., Sparta, M., Kesharwani, M. K., Martin, J. M. L., and Neese, F.: Exploring the Accuracy Limits of Local Pair Natural Orbital Coupled-Cluster Theory, J. Chem. Theory Comput., 11, 1525–1539, https://doi.org/10.1021/ct501129s, 2015.
- Link, M. F., Brophy, P., Fulgham, S. R., Murschell, T., and Farmer, D. K.: Isoprene versus Monoterpenes as Gas-Phase Organic Acid Precursors in the Atmosphere, ACS Earth Space Chem., 5, 1600–1612, https://doi.org/10.1021/acsearthspacechem.1c00093, 2021.
- Lu, T.: Molclus program, Version 1.10, http://www.keinsci.com/ research/molclus.html (last access: 1 July 2025), 2020.
- Lu, T. and Chen, F.: Multiwfn: A multifunctional wavefunction analyzer, J. Comput. Chem., 33, 580–592, https://doi.org/10.1002/jcc.22885, 2012.
- Mo, Z., Huang, S., Yuan, B., Pei, C., Song, Q., Qi, J., Wang, M., Wang, B., Wang, C., and Shao, M.: Tower-based measurements of NMHCs and OVOCs in the Pearl River Delta: Vertical distribution, source analysis and chemical reactivity, Environ. Pollut., 292, 118454, https://doi.org/10.1016/j.envpol.2021.118454, 2022
- Møller, K. H., Otkjær, R. V., Hyttinen, N., Kurtén, T., and Kjaergaard, H. G.: Cost-Effective Implementation of Multiconformer Transition State Theory for Peroxy Radical Hydrogen Shift Reactions, J. Phys. Chem. A, 120, 10072–10087, https://doi.org/10.1021/acs.jpca.6b09370, 2016.
- Müller, J.-F., Stavrakou, T., and Peeters, J.: Chemistry and deposition in the Model of Atmospheric composition at Global and Regional scales using Inversion Techniques for Trace gas Emissions (MAGRITTE v1.1) Part 1: Chemical mechanism, Geosci. Model Dev., 12, 2307–2356, https://doi.org/10.5194/gmd-12-2307-2019, 2019.
- Muthuramu, K., Shepson, P. B., and O'Brien, J. M.: Preparation, analysis, and atmospheric production of multifunctional organic nitrates, Environ. Sci. Technol., 27, 1117–1124, https://doi.org/10.1021/es00043a010, 1993.
- Neese, F.: The ORCA program system, WIREs Computational Molecular Science, 2, 73–78, https://doi.org/10.1002/wcms.81, 2012.
- Newland, M. J., Bryant, D. J., Dunmore, R. E., Bannan, T. J., Acton, W. J. F., Langford, B., Hopkins, J. R., Squires, F. A., Dixon, W., Drysdale, W. S., Ivatt, P. D., Evans, M. J., Edwards, P. M., Whalley, L. K., Heard, D. E., Slater, E. J., Woodward-Massey, R., Ye, C., Mehra, A., Worrall, S. D., Bacak, A., Coe, H., Per-

- cival, C. J., Hewitt, C. N., Lee, J. D., Cui, T., Surratt, J. D., Wang, X., Lewis, A. C., Rickard, A. R., and Hamilton, J. F.: Low-NO atmospheric oxidation pathways in a polluted megacity, Atmos. Chem. Phys., 21, 1613–1625, https://doi.org/10.5194/acp-21-1613-2021, 2021.
- Ohta, T.: Rate constants for the reactions of OH radicals with alkyl substituted olefins, Int. J. Chem. Kinet., 16, 879–886, https://doi.org/10.1002/kin.550160708, 1984.
- Parandaman, A., Kumar, M., Francisco, J. S., and Sinha, A.: Organic Acid Formation from the Atmospheric Oxidation of Gem Diols: Reaction Mechanism, Energetics, and Rates, J. Phys. Chem. A, 122, 6266–6276, https://doi.org/10.1021/acs.jpca.8b01773, 2018.
- Paulot, F., Wunch, D., Crounse, J. D., Toon, G. C., Millet, D. B., DeCarlo, P. F., Vigouroux, C., Deutscher, N. M., González Abad, G., Notholt, J., Warneke, T., Hannigan, J. W., Warneke, C., de Gouw, J. A., Dunlea, E. J., De Mazière, M., Griffith, D. W. T., Bernath, P., Jimenez, J. L., and Wennberg, P. O.: Importance of secondary sources in the atmospheric budgets of formic and acetic acids, Atmos. Chem. Phys., 11, 1989–2013, https://doi.org/10.5194/acp-11-1989-2011, 2011.
- Peng, J., Hu, M., Shang, D., Wu, Z., Du, Z., Tan, T., Wang, Y., Zhang, F., and Zhang, R.: Explosive secondary aerosol formation during severe haze in the North China Plain, Environ. Sci. Technol., 55, 2189–2207, https://doi.org/10.1021/acs.est.0c07204, 2021.
- Ren, H., Xia, Z., Yao, L., Qin, G., Zhang, Y., Xu, H., Wang, Z., and Cheng, J.: Investigation on ozone formation mechanism and control strategy of VOCs in petrochemical region: Insights from chemical reactivity and photochemical loss, Sci. Total Environ., 914, 169891, https://doi.org/10.1016/j.scitotenv.2024.169891, 2024.
- Riplinger, C., Sandhoefer, B., Hansen, A., and Neese, F.: Natural triple excitations in local coupled cluster calculations with pair natural orbitals, J. Chem. Phys., 139, https://doi.org/10.1063/1.4821834, 2013.
- Saunders, S. M., Jenkin, M. E., Derwent, R. G., and Pilling, M. J.: Protocol for the development of the Master Chemical Mechanism, MCM v3 (Part A): tropospheric degradation of non-aromatic volatile organic compounds, Atmos. Chem. Phys., 3, 161–180, https://doi.org/10.5194/acp-3-161-2003, 2003.
- Shaw, M. F., Sztáray, B., Whalley, L. K., Heard, D. E., Millet, D. B., Jordan, M. J. T., Osborn, D. L., and Kable, S. H.: Photo-tautomerization of acetaldehyde as a photochemical source of formic acid in the troposphere, Nat. Commun., 9, 2584, https://doi.org/10.1038/s41467-018-04824-2, 2018.
- Sommariva, R., Cox, S., Martin, C., Borońska, K., Young, J., Jimack, P. K., Pilling, M. J., Matthaios, V. N., Nelson, B. S., Newland, M. J., Panagi, M., Bloss, W. J., Monks, P. S., and Rickard, A. R.: AtChem (version 1), an open-source box model for the Master Chemical Mechanism, Geosci. Model Dev., 13, 169–183, https://doi.org/10.5194/gmd-13-169-2020, 2020.
- Srivastava, D., Vu, T. V., Tong, S., Shi, Z., and Harrison, R. M.: Formation of secondary organic aerosols from anthropogenic precursors in laboratory studies, npj Clim. Atmos. Sci., 5, 22, https://doi.org/10.1038/s41612-022-00238-6, 2022.
- Srivastava, D., Li, W., Tong, S., Shi, Z., and Harrison, R. M.: Characterization of products formed from the oxidation of toluene and m-xylene with varying

- NO_x and OH exposure, Chemosphere, 334, 139002, https://doi.org/10.1016/j.chemosphere.2023.139002, 2023.
- Tan, Z., Lu, K., Jiang, M., Su, R., Wang, H., Lou, S., Fu, Q., Zhai, C., Tan, Q., Yue, D., Chen, D., Wang, Z., Xie, S., Zeng, L., and Zhang, Y.: Daytime atmospheric oxidation capacity in four Chinese megacities during the photochemically polluted season: a case study based on box model simulation, Atmos. Chem. Phys., 19, 3493–3513, https://doi.org/10.5194/acp-19-3493-2019, 2019.
- Tan, Z., Feng, M., Liu, H., Luo, Y., Li, W., Song, D., Tan, Q., Ma, X., Lu, K., and Zhang, Y.: Atmospheric Oxidation Capacity Elevated during 2020 Spring Lockdown in Chengdu, China: Lessons for Future Secondary Pollution Control, Environ. Sci. Technol., 58, 8815–8824, https://doi.org/10.1021/acs.est.3c08761, 2024.
- Tuazon, E. C., Aschmann, S. M., Arey, J., and Atkinson, R.: Products of the Gas-Phase Reactions of a Series of Methyl-Substituted Ethenes with the OH Radical, Environ. Sci. Technol., 32, 2106–2112, https://doi.org/10.1021/es980153a, 1998.
- Wang, N., Kostenidou, E., Donahue, N. M., and Pandis, S. N.: Multi-generation chemical aging of α-pinene ozonolysis products by reactions with OH, Atmos. Chem. Phys., 18, 3589–3601, https://doi.org/10.5194/acp-18-3589-2018, 2018.
- Wang, S., Newland, M. J., Deng, W., Rickard, A. R., Hamilton, J. F., Muñoz, A., Ródenas, M., Vázquez, M. M., Wang, L., and Wang, X.: Aromatic Photo-oxidation, A New Source of Atmospheric Acidity, Environ. Sci. Technol., 54, 7798–7806, https://doi.org/10.1021/acs.est.0c00526, 2020.
- Wang, S., Zhao, Y., Han, Y., Li, R., Fu, H., Gao, S., Duan, Y., Zhang, L., and Chen, J.: Spatiotemporal variation, source and secondary transformation potential of volatile organic compounds (VOCs) during the winter days in Shanghai, China, Atmos. Environ., 286, 119203, https://doi.org/10.1016/j.atmosenv.2022.119203, 2022.
- Wu, R. and Xie, S.: Spatial Distribution of Secondary Organic Aerosol Formation Potential in China Derived from Speciated Anthropogenic Volatile Organic Compound Emissions, Environ. Sci. Technol., 52, 8146–8156, https://doi.org/10.1021/acs.est.8b01269, 2018.
- Wu, R., Vereecken, L., Tsiligiannis, E., Kang, S., Albrecht, S. R., Hantschke, L., Zhao, D., Novelli, A., Fuchs, H., Tillmann, R., Hohaus, T., Carlsson, P. T. M., Shenolikar, J., Bernard, F., Crowley, J. N., Fry, J. L., Brownwood, B., Thornton, J. A., Brown, S. S., Kiendler-Scharr, A., Wahner, A., Hallquist, M., and Mentel, T. F.: Molecular composition and volatility of multi-generation products formed from isoprene oxidation by nitrate radical, Atmos. Chem. Phys., 21, 10799–10824, https://doi.org/10.5194/acp-21-10799-2021, 2021.
- Yang, J., Zeren, Y., Guo, H., Wang, Y., Lyu, X., Zhou, B., Gao, H., Yao, D., Wang, Z., Zhao, S., Li, J., and Zhang, G.: Wintertime ozone surges: The critical role of alkene ozonolysis, Environ. Sci. Ecotechnol., 22, 100477, https://doi.org/10.1016/j.ese.2024.100477, 2024.
- Yang, Y., Guo, W., Sun, J., Chen, Q., Meng, X., Wang, L., Tao, H., and Yang, L.: Characteristics of volatile organic compounds and secondary organic aerosol pollution in different functional areas of petrochemical industrial cities in Northwest China, Sci. Total Environ., 858, 159903, https://doi.org/10.1016/j.scitotenv.2022.159903, 2023.
- Zádor, J., Fernandes, R. X., Georgievskii, Y., Meloni, G., Taatjes, C. A., and Miller, J. A.: The reaction of hydrox-

- yethyl radicals with O₂: A theoretical analysis and experimental product study, P. Combust Inst., 32, 271–277, https://doi.org/10.1016/j.proci.2008.05.020, 2009.
- Zeng, L., Yang, B., Xiao, S., Yan, M., Cai, Y., Liu, B., Zheng, X., and Wu, Y.: Species profiles, in-situ photochemistry and health risk of volatile organic compounds in the gasoline service station in China, Sci. Total Environ., 842, 156813, https://doi.org/10.1016/j.scitotenv.2022.156813, 2022.
- Zhao, Y. and Truhlar, D. G.: The M06 suite of density functionals for main group thermochemistry, thermochemical kinetics, non-covalent interactions, excited states, and transition elements: two new functionals and systematic testing of four M06-class functionals and 12 other functionals, Theor. Chem. Acc., 120, 215–241, https://doi.org/10.1007/s00214-007-0310-x, 2008.
- Zheng, J., Bao, L. J., Meana-Pañeda, R., Zhang, S., Lynch, B. J.,
 Corchado, J. C., Chuang, Y.-Y., Fast, P. L., Hu, W.-P., Liu, Y.-P.,
 Lynch, G. C., Nguyen, K. A., Jackels, C. F., Fernandez Ramos,
 A., Ellingson, B. A., Melissas, V. S., Villà, J., Rossi, I., Coitiño,
 E. L., Pu, J., Albu, T. V., Ratkiewicz, A., Steckler, R., Garrett, B.
 C., Isaacson, A. D., and Truhlar, D. G.: Polyrate-version 2017-C,
 University of Minnesota, Minneapolis, MN, https://comp.chem.
 umn.edu/polyrate/ (last access: 9 November 2024), 2018.